Synthesis of Super-Hydrophobic Polymer Nanocomposites as a Smart Self-Cleaning Coating Films

Saber Ibrahim,[1] Ahmad Labeeb,[2,3] Ahmed F. Mabied,[4] Omar Soliman,[1] Azza Ward,[2] Salwa L. Abd-El-Messieh,[2] Abouelfotouh A. Abdelhakim[1]

[1]*Packaging Materials Department, National Research Centre, Elbuhoth Street 33, Dokki, Cairo, 12311, Egypt*

[2]*Microwaves Physics and Dielectrics Department, National Research Centre, Elbuhoth Street 33, Dokki, Cairo, 12311, Egypt*

[3]*Liquid Crystal Institute, Chemical Physics Interdisciplinary Program, Kent State University, Kent, Ohio, 44242*

[4]*Solid State Physics Department, National Research Centre, Elbuhoth Street 33, Dokki, Cairo, 12311, Egypt*

Super-hydrophobic (SH) surfaces have garnered significant attention due to their potentially diverse range of applications (e.g., self-cleaning surfaces, waterproof fabrics, non-stick containers, and microfluidics). The manufacturing methods of SH surfaces are generally expensive and often require specialized tools. In this study, we employed simplified production methods, and we focused on cheap chemical modification of common polymers using nanocomposites to create SH surfaces. Polymer nanocomposites have many advantages as a coating by increasing volume/area of nanoparticles. Coating clarity, surface hydrophobicity, roughness, electrical properties, and crystallinity are some unique behaviors of nanocomposites. We studied the physical properties of these chemically modified polymers to explore the acquired SH property. We investigated SH films using many techniques such as size-exclusion chromatography (SEC), X-ray diffraction (XRD), differential scanning calorimetry (DSC), scanning electron microscopy (SEM), transmission electron microscopy (TEM), and dynamic light scattering (DLS). Our goal was to verify that these materials could be used as SH films that acted as cleaned, solid surfaces in direct contact with packaging surfaces. POLYM. COMPOS., 00:000–000, 2016. © 2016 Society of Plastics Engineers

INTRODUCTION

Many types of polymers can be used for packaging food, tools, and other items. These polymers can be translated, placed on shelf storage in open air, and used in dirty places or in a vapor atmosphere (e.g., chairs in stadiums or cars). These conditions accelerate the attachment of dirty, small particles of sand or other undesirable materials to render the surface unclean and visually unappealing. Furthermore, outside windows or doors need to be cleaned daily. Therefore, it is necessary to prepare special types of polymer characteristics with self-cleaning behaviors to overcome this vital problem.

Wettability is an important property of solid surfaces and is mainly determined by two factors: the surface topography and chemical composition [1–12]. Super-hydrophobic (SH) surfaces [3–9, 13–18], which have a contact angle (CA) larger than 150°, have attracted much attention due to their practical applications [19]. Super-hydrophobic surfaces can usually be achieved by forming hierarchical micro/nanoscale binary structures and by chemical modification to apply materials with low surface energy to another material. The Wenzel model [1] and the Cassie-Baxter model [12] are most frequently used to account for experimental results. The Wenzel model describes wetting behavior where a liquid droplet on a rough surface is in intimate contact with surface asperities, while the Cassie model describes states where the droplet sits on a solid–air composite surface [20–25]. The key difference between the two regimes is the contact angle hysteresis, with the contact angle hysteresis of the Cassie wetting regime being much lower than that of the Wenzel wetting regime.

Correspondence to: S. Ibrahim; e-mail:saberam2000@yahoo.com
Contract grant sponsor: National Research Centre, Egypt; contract grant number: 10050405.
DOI 10.1002/pc.24023
Published online in Wiley Online Library (wileyonlinelibrary.com).

The underlying trapped air in a Cassie state can be eliminated when a pressure is applied, resulting in a transition to the Wenzel state. This is called a "metastable" Cassie state. The contact mode depends on the way liquid drops are deposited on the surface. For example, dragging over a rough surface [26] or being impacted can lead to such a transition [27]. The impact action of a droplet on a super-hydrophobic surface has been studied by several groups [28–37].

Lee and coworkers [27] confirmed that the impacting action between water droplets and the surface depends on the geometric parameters of the surface, and only certain geometries could result in a robust Cassie regime [27]. Bhushan and coworkers [29] developed a criterion in which the transition from the Cassie regime to the Wenzel regime is determined by three factors: impact velocity, geometric parameters of patterned surfaces (the length, width, and height of patterns and pitch between them), and liquid properties. Generally, the mentioned studies focus on the effect of geometric parameters of surfaces on the wetting mode [38]. The present study shows that the surface composition in low fractions might not affect the surface wettability, but the surface wetting transitions and contact angle hysteresis can be altered significantly by manipulating the droplet–surface interaction, which has never been reported before. We demonstrate the dynamic wetting behavior of a pressed water droplet on anodized alumina, which was modified with responsive polymer brushes after pretreatment with a dilute initiator [39]. The wetting transition between super hydrophobicity and hydrophilicity may be achieved depending on the responsiveness between droplets of different pH, the concentrations of electrolytes, the environmental temperature, and surface-grafted stimuli-responsive polymer brushes. The distinct CA changes give the surface double-faced wetting characteristics.

The general aim of this research is developing a super-hydrophobic surface by a sol–gel polymerization method involving suitable polymers of different types with various functionalities. Inorganic particles and metal oxides help these polymers to develop super-hydrophobicity and substantially increase the self-cleaning functionality of currently available surfaces. These developments include fast cleaning and faster super drying with the highest quality of the overall surface. Hopefully, these developments will lead to commercially available super-hydrophobic surface materials.

A dielectric materials measurement can provide critical design parameter information form any applications. For example, the loss of a cable insulator, the impedance of a substrate, or the frequency of a dielectric resonator. This information is also useful for improving packaging designs. More recent applications in the area of industrial microwave processing of food, rubber, plastic, and ceramics have also were found to benefit from knowledge of dielectric properties. Hydrophobicity of insulating materials is treated as the resistance to formation of conducting water tracks that increase leakage current, chances of flashover, and other deterioration effects. The superior performances of polymer outdoor insulating materials are regarded as the contribution of their hydrophobic surfaces.

Super-hydrophobic surfaces were made by mini-emulsion formation through sophisticated polymerization techniques and by comparison with natural hydrophobic surfaces. The super-hydrophobic polymers were doped by stabilized inorganic particles to boost the super-hydrophobic performance of the surfaces using metal alkoxides (SiO_2 and with silica/chlorotrimethylsilane, SiO_2/CTMS) as a requirement for super-hydrophobicity. Multilayer samples with a modified organic–inorganic top layer could produce water contact angles of up to 130°.

MATERIALS AND METHODS

Materials

Styrene, Sigma-Aldrich, was purified before being used. Chlorotrimethylsilane (CTMS) and sodium silicate, Sigma-Aldrich, were used as silica precursors. Potassium peroxide sulfate, sodium bicarbonate, hexadecane (HD), hydroquinone (HQ), and sodium dodecyl sulfate (SDS) were obtained from Sigma-Aldrich and were used as received.

Methods

Preparation and Chemical Modification of Hydrophobic Silicon Precursor Nanoparticles. Silica (SiO_2) nanoparticles were prepared by the hydrolysis reaction of sodium silicate (17.4 g), which was dissolved in 300 ml of deionized water, followed by the addition of 100 ml of 0.24 M NH_4Cl solution. The solution was stirred for 3 h at 80°C. After that, the white product was filtered and washed with deionized water and alcohol until Cl^- could not be detected. Subsequently, the SiO_2 nanoparticles were chemically modified by CTMS. The white product and 0.05 moles of CTMS were dissolved in 200 mL of alcohol, the mixture was heated to 80°C, and stirred for 3 h. After reaction, the resulting product was filtered and dried in a vacuum at room temperature for 24 h to obtain CTMS-functionalized SiO_2 powder. Polystyrene (PS)-encapsulated silicone dioxide nanoparticles were prepared through a mini-emulsion polymerization technique.

Synthesis of Hydrophobic Polymer Coating. Three-neck tube, a specified amount of monomer styrene and 0.031 moles of hydrophobe (hexadecane, HD) were added to a solution containing 0.024 sodium dodecyl sulfate (SDS) in 71.28 g of water. The mixture was degassed (vac/N_2, followed by stirring for 30 min under N_2 at 100 min^{-1}) and then stirred for 1.0 h at 800 rpm. After that, a mini-emulsion was prepared by ultrasonication for 11 min (90% amplitude) with an ultrasonic disintegrator (Branson

 DOI 10.1002/pc

450W). A slight stream of nitrogen was applied and the emulsion was cooled with ice water.

Different amounts of SiO_2 modified with CTMS were dispersed in 22 ml of water using a sonicator for 5 min at 25% amplitude and were added to the reaction mixture. The formed mini-emulsion was transferred to the reaction vessel. After short degassing, the temperature was raised to 72°C. Then, an aqueous solution of initiator was added (360 mg of potassium persulfate (KPS) in 7.2 g of water degassed under N_2 for 30 min). The reaction was performed at 800 rpm for 4 h and then the mixture was cooled to 25°C. The reaction vessel was immersed in an ice bath to decrease the temperature until room temperature. The dispersion was precipitated in 300 mL of MeOH (1 wt% HQ) and the precipitation was done by adding latex solution drop wise. Polystyrene was filtrated and dried in a vacuum oven overnight.

Sample Preparation for Dynamic Light Scattering (DLS). About 250 mg of latex was added to 20 g of Millipore water (containing 0.1 wt% SDS and 0.1 wt% HQ relative to Millipore water) and the mixture was stirred for 30 min at room temperature.

Transmission Electron Microscopy (TEM) Investigation. Polymer and nanocomposite materials were prepared by dropping a solution on a carbon-coated copper grid (S160-3 Plano GmbH) and investigated using a JEOL 120/JEOL 200 TEM (Carl Zeiss NTS) operated at 120 kV/200 kV. Zero-loss energy filtering was used to increase the image contrast. The size distribution of the particles was determined by an automatic particle-identification routine in Scandium software.

X-Ray Diffraction (XRD). A fine powder of the studied samples was used for X-ray diffraction (XRD) measurements. The data were collected at ambient temperature using a computer-controlled X-ray diffractometer (PAN analytical Empyrean) with Cu kα radiation (λ kα = 1.5406 Å) operated at 30 mA and 45 kV. The powder diffraction patterns were scanned in the 2Θ range of 4–50° with a scan step of 0.026° and counting time of 100 s/step. A quartz standard sample was used to determine the zero shifts and the instrumental profile under the same data collection conditions. The crystallinity index was calculated using Win Fit software using Lorentz correction as background [40].

Dielectric Spectroscopy Technique. For dielectric measurements, thin films were prepared through a solution casting technique. Dielectric and conductivity measurements were carried out using a high-resolution broadband impedance analyzer (Schlumberger Solartron 1260). The frequency range of the applied AC electric field was between 0.1 Hz and 1 MHz. Good electromagnetic shielding was implemented for the whole sample holder in order to reduce noise problems that are especially common at low frequencies. The measurements were automated by interfacing the impedance analyzer with a personal computer through an IEE488 GPIB cable. The commercial interfacing and automation software LabVIEW was used for acquisition of data. The complex permittivity ε^* consists of a real part ε' which is related to the stored energy within the medium and an imaginary part ε'' which is related to the dissipation (or loss) of energy within the medium. The following notation is used for the complex permittivity ε^* ($\varepsilon^* = \varepsilon' + \varepsilon''$). Both ε' and ε'' are calculated based on equations $\varepsilon' = Cd/\varepsilon_o A$ and $\varepsilon'' = \varepsilon' \tan\delta$, where C is capacitance of the dielectric, d thickness of the sample which its range is 170–220 μm, A is area of electrode, and ε_o is permittivity of vacuum (8.85×10^{-12} F/m). Calculation of the permittivity is performed by dividing the capacitance of the cell with dielectric material C to capacitance of empty cell C_o, where $\varepsilon' = C/C_0$. Capacitance (C) and tanδ values are obtained directly from high-resolution broadband impedance analyzer (Schlumberger Solartron 1260). The calculations are made automatically by LabVIEW 7.1 software. The errors in ε' and ε'' were 1% and 3%, respectively. The temperature of the samples was controlled by a temperature regulator with a Pt 100 sensor. The error in temperature measurements was ±0.5°C. To avoid moisture, the samples were stored in desiccators with silica gel. Thereafter, the samples were transferred to a measuring cell and left with P_2O_5 until the measurements were carried out.

RESULTS AND DISCUSSION

Contact Angle Measurements

The wetting behavior was studied via contact angle measurement of polystyrene and polystyrene-loaded silica with different ratios (from 2 up to 10 wt%), as shown in Fig. 1. The polystyrene loaded with silica nano-particles shows non-wetting surfaces where water droplets become more non-wettable than the unloaded polystyrene sample. Although there are gradual decreases in measured contact angles with time for all samples around 7°, there are significant increases (20°) with increasing weight percentage of silica nano-particles. Consequently, increasing the silica loading in the polymer results in more non-wettable surfaces (high contact angle).

Particle Size Investigation

Dynamic light scattering (DLS) can be considered as a main tool to understand and verify models pertaining to the dynamics of polymers in dilute solution. It determines the size and hydrodynamic radius of polymer molecules in solution. Silica nanoparticles were prepared through hydrolysis and condensation reactions of silane precursor in the presence of CTMS, as described previously. Then, a sol–gel of silicon nanoparticles was added with different

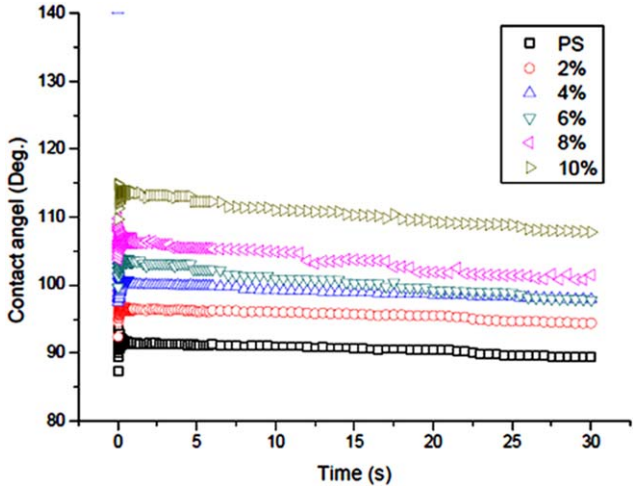

FIG. 1. The change in contact angle of polystyrene PS and PS encapsulated modified SiO_2 at different ratios with time. [Color figure can be viewed in the online issue, which is available at wileyonlinelibrary.com.]

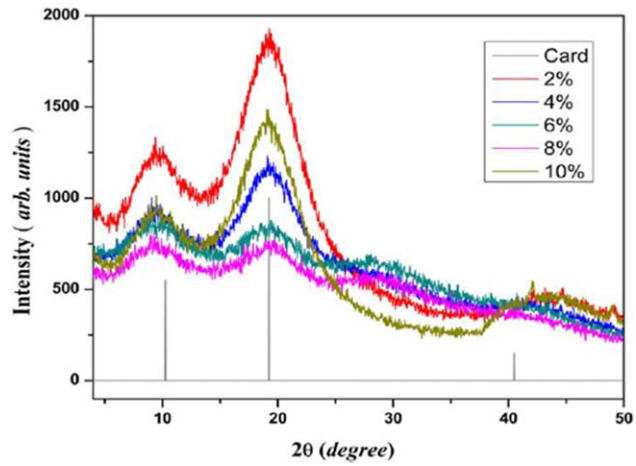

FIG. 3. X-ray diffraction patterns of polystyrene (PS) with different amounts of silica nano-particles (2%, 4%, 6%, 8%, and 10%), including the reference card of PS. [Color figure can be viewed in the online issue, which is available at wileyonlinelibrary.com.]

ratios during the mini-emulsion polymerization reaction of styrene monomer. Figure 2 shows a narrow polydispersity index (PDI) of particle size distribution as a uni-model diameter. The diameters of the silica nano-particles were determined by DLS to be in the range of 60–70 nm.

XRD Analysis

XRD results in Fig. 3 show that polystyrene particles with the different amounts of silica nano-particles are well defined according to card no. 00-060-1507 of the The International Center for Diffraction Data (ICDD) database (PDF-2, 2010). The diffraction peak positions of 10.25°, 19.22°, and 40.58° are detected in all samples. The diffraction patterns indicate that polystyrene/silica composites were in the same matrix since distinct crystal-

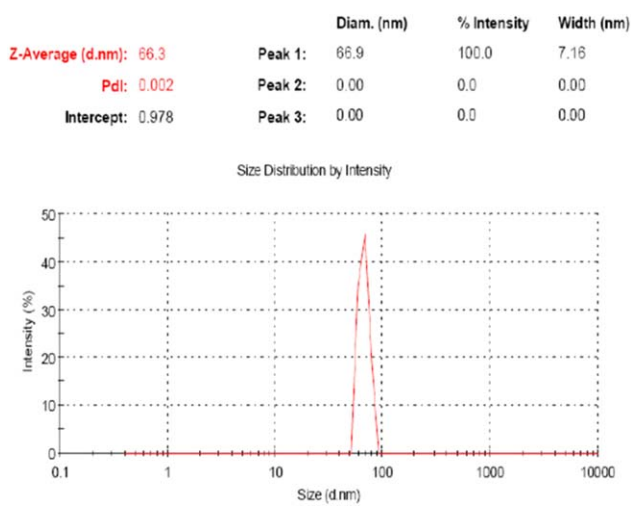

FIG. 2. DLS band of polystyrene/10% (SiO_2/CTMS) by mini-emulsion polymerization techniques. [Color figure can be viewed in the online issue, which is available at wileyonlinelibrary.com.]

line peaks of silica did not appear. This means there is no phase separation between the polystyrene and silica nano-particles.

The crystallinity index of the samples was calculated considering the peak at 19.2° as the reference crystalline peak, as shown in Fig. 3. The crystallinity index calculation was done using the area under the peaks based on the profile fitting to eliminate the instrumental error [40].

The crystallinity index decreases with increase in the amount of silica to 6% and then increases at 8% and 10% silica (Table 1). This could mean that the sample rearrangement prefers to be in the crystalline form after a certain amount of aggregation of silica nano-particles.

TEM Investigations

The polystyrene and polystyrene/modified silica nanocomposites were studied as a model for hydrophobic coating. Encapsulation reaction for different ratios of modified silica was carried out through *in-situ* mini-emulsion polymerization reaction. Figure 4 shows transmission electron microscopy (TEM) micrographs of the modified silica nanoparticles with CTMS at different magnifications. The polystyrene was polymerized in the presence of CTMS at different ratios as a silicon source. Most of the micrographs show particles with very good circularity and a smooth surface with low distribution of the particle size in the range of 60–70 nm.

From the results of DLS and TEM, it can be concluded that there is a uni-model band with narrow distribution range. Most of the Brownian motion particles have

TABLE 1. Crystallinity index of PS/SiO_2 nanocomposites

Sample	2%	4%	6%	8%	10%
Crystallinity index	79%	69%	38%	42%	81%

DOI 10.1002/pc

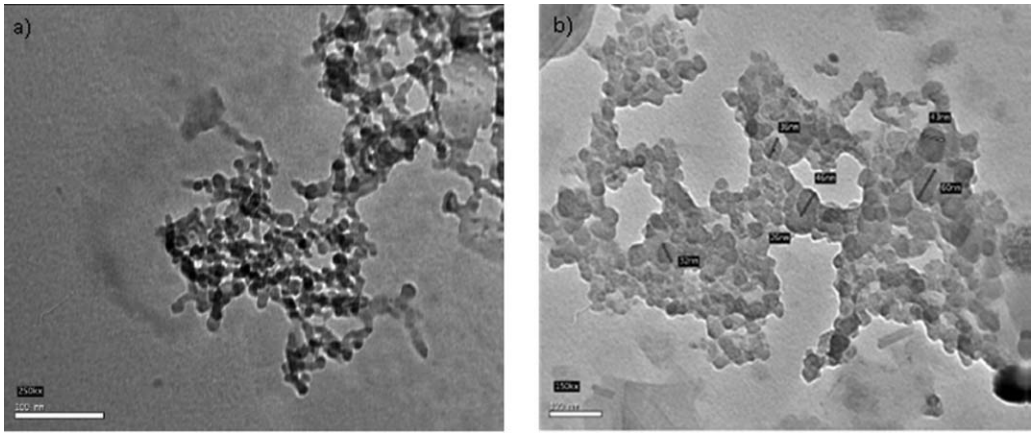

FIG. 4. TEM micrographs the PS/CTMS nanoparticles with different magnifications.

average particle size of 66 nm with low PDI of 0.002. Micrographs of silicon oxide modified with CTMS are presented in Fig. 5. Modified silica nanoparticles appeared as an aggregated silicon oxide sol–gel. Most of the examined particles showed average particle size of 30 to 60 nm.

As represented in Figs. 2 and 4, there is good agreement in the particle size measurements between DLS and TEM for polystyrene nano-composites (66 nm and 70 nm, respectively). The reduction of particle size in aqueous solution during DLS measurement can be explained by the hydrophobicity of the homogenous polymer spheres.

Dielectric Properties

The dielectric properties are shown in Fig. 6 and represent the permittivity ε' and dielectric loss ε'' versus the applied frequency for polystyrene and CTMS at different temperatures covering the range before and after the glass transition temperature of polystyrene (~100°C). The permittivity and dielectric loss were measured over a frequency range 0.1 Hz to 1 MHz and temperature range of 20 to 120°C. Examples of the obtained data for polystyrene with 4 wt% SiO_2 and 10 wt% SiO_2 at different temperatures are illustrated in Fig. 6a and b. It is clear that the values of ε' decreased with increasing frequency and showed anomalous dispersion. The rotational motion of the polar molecules of dielectric is not sufficiently rapid to attain equilibrium with the field [41]. This behavior is expected in most dielectric materials, which is attributed to the dielectric relaxation phenomena of the materials among them polymers. Within the measured frequency range, the dielectric relaxation involves the dipolar (rotational) polarization, which depends on the molecular structure of the material. At higher frequencies, the rotational motion of the molecules lag behind the electric field and consequently the permittivity reduced with increasing frequency [41].

The decrease in ε'' values with frequency is related to dispersion and polarization processes. Comparing Fig. 6a and b indicates that the values of ε' and ε'' are affected by the increase of silica content. This may be due to the fact that the silane modification reduces the number of silanol groups, which are highly polar as well as the number of charge carriers [42].

In the same figures, the dielectric dispersion (ε'') is quite broad, even broader than the predicted values by

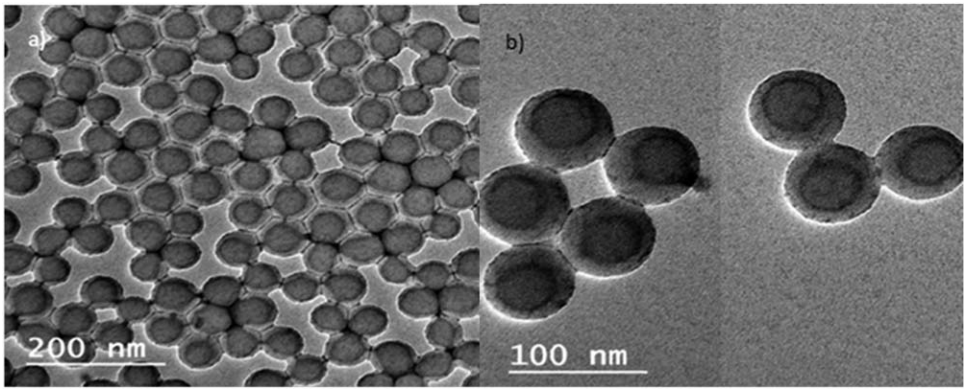

FIG. 5. TEM micrographs of SiO_2/CTMS nanoparticles with magnification (a) 150 K and (b) 250 K.

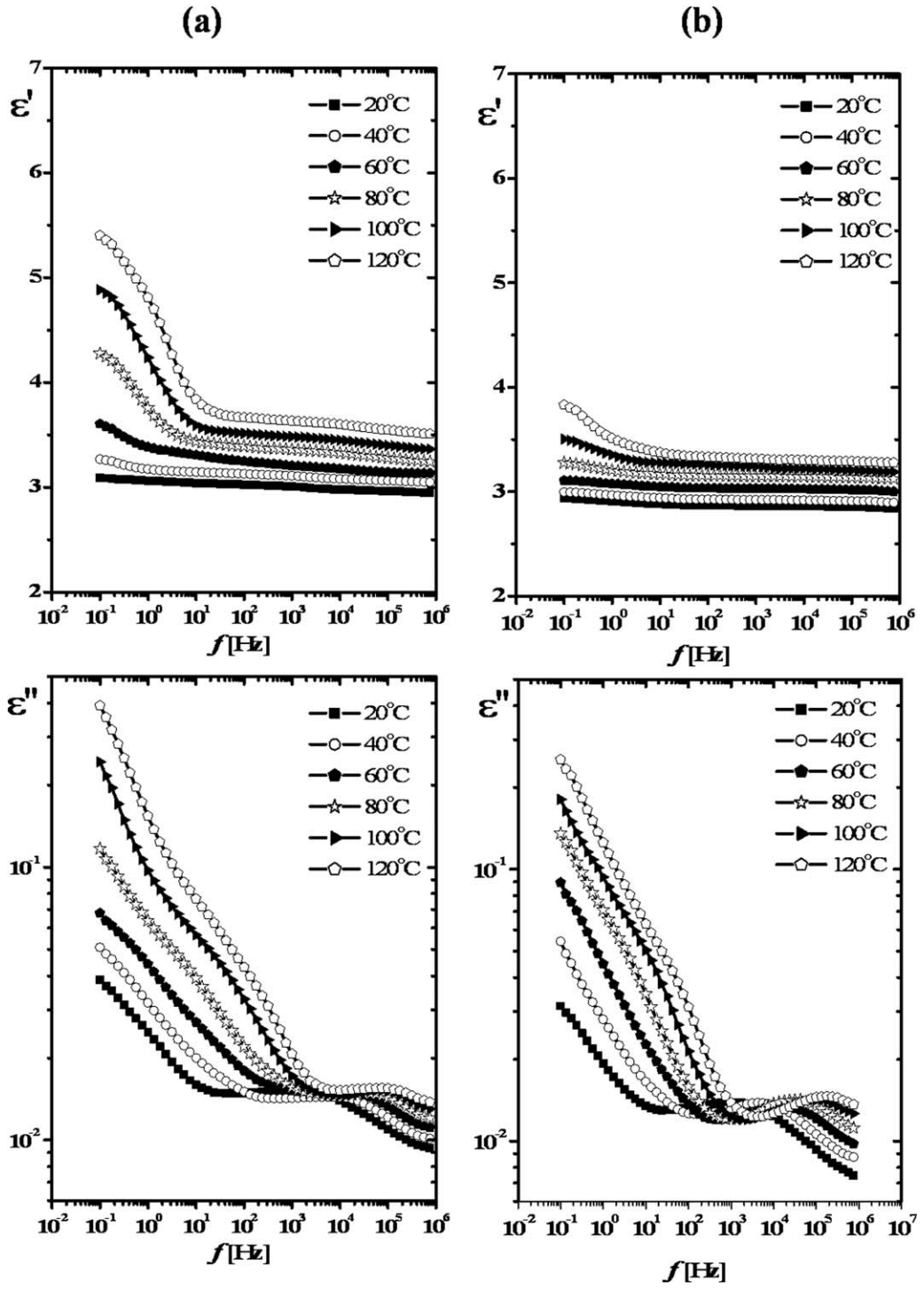

FIG. 6. The frequency dependence of permittivity ϵ' and dielectric loss ϵ" for PS on concentration of silica (SiO_2), where (a) PS-4 wt% SiO_2 and (b) PS-10 wt% SiO_2.

Debye theory [43]. Moreover, the spectra of ε'' shows that in addition to DC conductivity, more than one relaxation mechanism is expected. The conductivity contribution for the dielectric loss was described by:

$$\varepsilon''_{\sigma} = \sigma_{dc}/\varepsilon_o \omega$$

where σ_{dc} is the conductivity and $\varepsilon_o = 8.854 \times 10^{-12}$ F/m is the permittivity of vacuum.

Figure 7 shows the variation of permittivity (ε') and dielectric loss (ε'') of polystyrene composites with SiO_2 content at a fixed frequency and room temperature (~20°C). The values of both ε' and ε'' initially increased up to 6 wt% SiO_2 and then decreased with the SiO_2 content. The increase in ε' and ε'' with increasing silica nanoparticles is due to the lower values of ε' and ε'' of pure polystyrene (2.4–2.7) [44] than that of silica (3.9–4)

 DOI 10.1002/pc

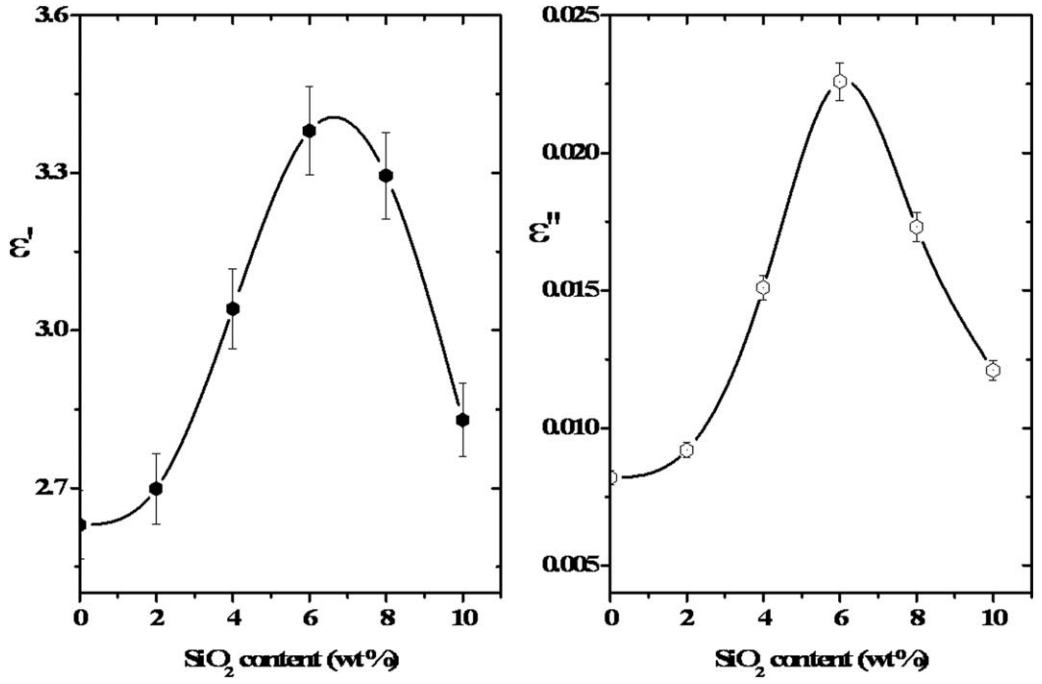

FIG. 7. Dependence of permittivity ϵ' and dielectric loss ϵ" for PS on concentration of silica (SiO_2).

[45]. Moreover, this increase in both values may be due to the presence of a number of silanol groups, which are highly polar, as well as the number of charge carriers. In addition, the filler loading increase the density of the system. This in turn reduced the orientation of the dipoles, which is the cause of the noticed decrease in both values [46].

Figure 8 shows that both ε′ and ε″ increase with temperature. This enhancement is attributed to the increasing charge carrier mobility. In addition, as the temperature

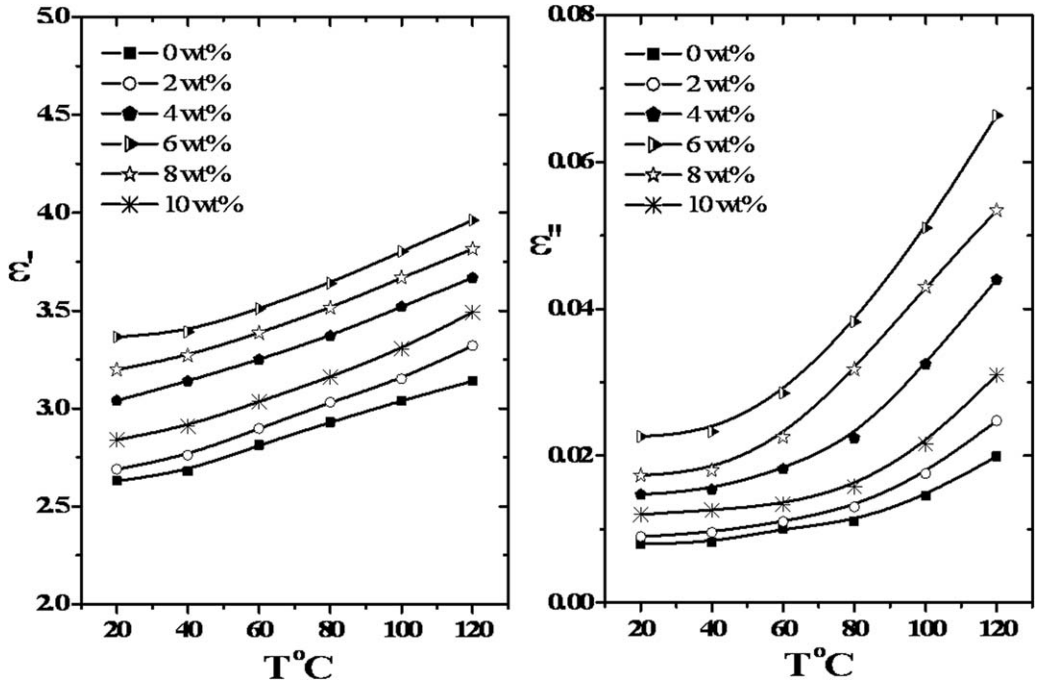

FIG. 8. Dependence of permittivity ϵ' and dielectric loss ϵ" for PS and PS/(CTMS/SiO_2) composites on temperature.

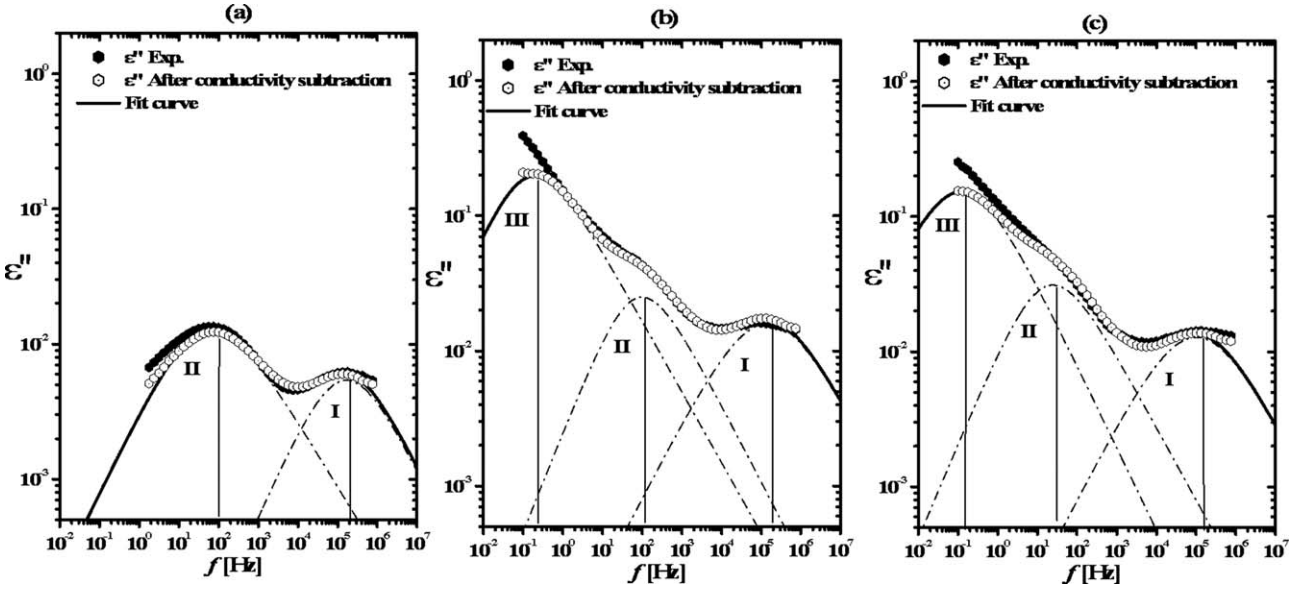

FIG. 9. The dielectric loss ϵ" versus the frequency f (Hz) for polystyrene (PS) with different concentration of silica. (a) Pure PS, (b) PS-4 wt% SiO_2, and (c) PS-10 wt% SiO_2 decomposition of ϵ" into three relaxation processes after conductivity subtraction at 120°C.

increases, the orientation of dipoles is facilitated, which enhances both ε′ and ε″.

The experimental data for ε″ were analyzed using a computer program based on superimposed HavriliakNagami [47]. The dielectric spectra include most of the dielectric relaxations observed in the polystyrene composites. The obtained data are illustrated graphically in Fig. 9. For the pure polystyrene sample (Fig. 9a), the data after DC conductivity subtraction are represented by two absorption regions. The dielectric loss spectra thus show two maximums. The first one seen at high frequency (I) may be attributed to β-relaxation due to the orientation of the side groups attached to the main chain. The position of the peak of the β-process is not much affected by the increase of the silica content.

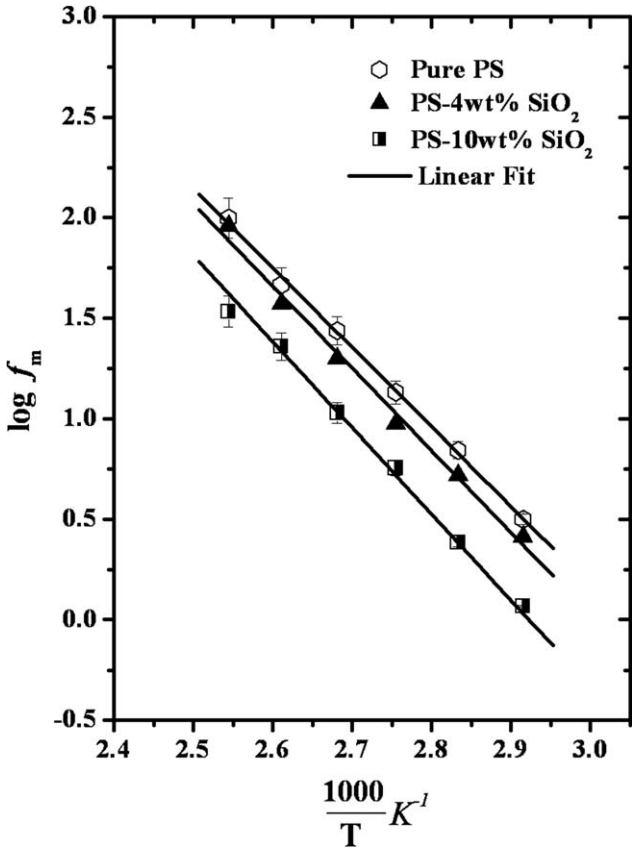

FIG. 10. Dependence of relaxation time τ (process II) for polystyrene (PS)/silica composites on silica content.

The lower frequency relaxation (II) could be due to the relaxation of the main chain [43, 48]. However, the same processes are found for the filled samples (Fig. 9b and c) in addition to a third relaxation (III). The third relaxation (III) could be attributed to the Maxwell-Wagner-Sillars effect (MWS) [49, 50], which originates from an AC current that is in phase with the applied potential. The differences in conductivities and permittivity of the substances are composing the dielectric properties. However, the high dielectric loss of this process originates from charge carriers like ions, the motion of which is limited by interfaces.

The temperature dependence of the relaxation process is further analyzed by plotting the frequency of the maximum versus the reciprocal of temperature. From Fig. 10, it is clear that the frequency of the maximum increased at higher temperatures due to enhancement of mobility of charge carriers at high temperature. This temperature dependence of dielectric relaxation can be well described by Arrhenius type behavior (see Fig. 10). The plots for the relaxation processes yield a straight line and from the slope of the line, the activation energy can be calculated using the following Arrhenius equation:

 DOI 10.1002/pc

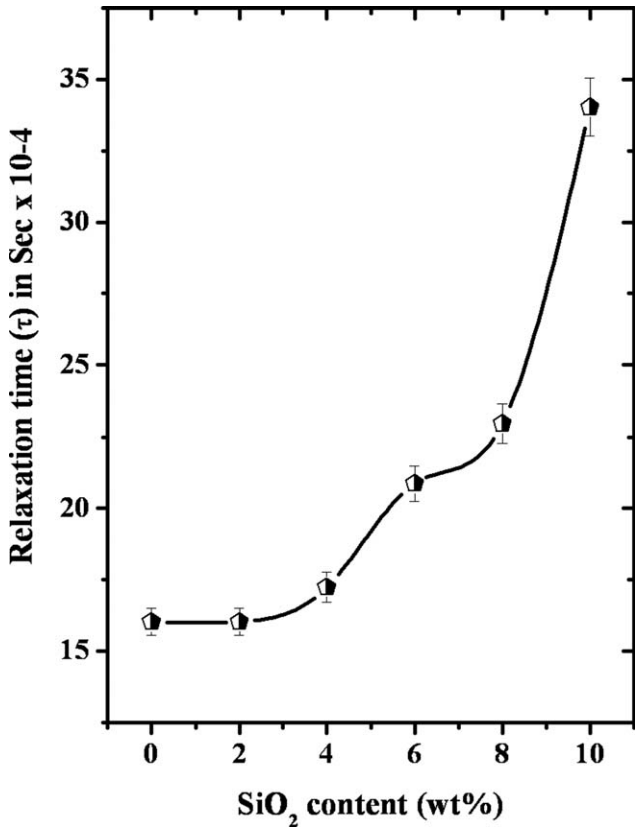

FIG. 11. Relaxation time for the relaxation processes (II) with respect to the silica content.

$$f = f_o \exp\left[\frac{-E_A}{k\ T}\right]$$

where E_A is the activation energy, f_0 is the pre-exponential factor, k is the Boltzmann constant, and T is the absolute temperature. The calculated activation energies of processes II (at intermediate frequency) were found to be about 32.91–35.71 kJ/mol. The highest value of the activation energy of the this process is a clear indication that some sort of interaction between PS molecules and SiO_2 took place. These interactions can be responsible for restricting the motion of polymer chains in their surrounding environment, thus lowering the mobility of the PS macromolecular segments, whereas the relaxation processes shifted to lower frequency by incorporating SiO_2 to PS matrix (see Fig. 9)

Moreover, the analysis results regarding relaxation time (τ) for the relaxation processes (II) are illustrated in Fig. 11 with respect to the silica content. The relaxation time (τ) is increased with increasing silica contents as in Fig. 10. This increase may be due to the decrease in the degrees of freedom by increasing the filler content as in Fig. 11 [51].

CONCLUSION

A PS/SiO_2 nanocomposite coating was prepared through mini-emulsion polymerization encapsulation technique. Contact angle measurement of the polymer nanocomposite coating film indicated a high value that is recommended for self-cleaning super-hydrophobic coatings. The XRD patterns were confirmed the presence of silica (SiO_2) nanoparticles in the matrix of polystyrene (PS). The dielectric properties were characterized for the hydrophobic polystyrene/silica mixtures. The permittivity ε' and dielectric loss ε'' decreased with increasing silica contents due to the wettability of silica and PS. As the concentration of silica increased, the orientation of the dipoles reduced and caused a decrease in both the permittivity and loss values. Moreover, ε' and ε'' increased with temperature. These enhancements were regarded to result from the increase of the charge carrier mobility. From the dielectric spectra, it can be concluded that the relaxations of the polymer mixtures depend on the silica content and wettability of the hydrophobic polystyrene/silica mixtures.

REFERENCES

1. R.N. Wenzel, *Ind. Eng. Chem.*, **28**, 988 (1936).
2. A.B.D. Cassie and S. Baxter, *Trans. Faraday Soc.*, **40**, 546 (1944).
3. T. Onda, S. Shibuichi, N. Satohand, and K. Tsujii, *Langmuir*, **12**, 2125 (1996).
4. S. Shibuichi, T. Onda, N. Satoh, and K. Tsujii, *J. Phys. Chem.*, **100**, 19512 (1996).
5. W. Chen, A.Y. Fadeev, M.C. Hsieh, D. Oner, J. Youngblood, and T.J. McCarthy, *Langmuir*, **15**, 3395 (1999).
6. D. Oner and T.J. McCarthy, *Langmuir*, **16**, 7777 (2000).
7. L. Feng, S. Li, Y. Li, H. Li, L. Zhang, J. Zhai, Y. Song, B. Liu, L. Jiang, and D. Zhu, *Adv. Mater.*, **14**, 1857 (2002).
8. L. Feng, S.H. Li, H.J. Li, J. Zhai, Y.L. Song, L. Jiang, and D.B. Zhu, *Angew. Chem., Int. Ed.*, **41**, 1221 (2002).
9. H.Y. Erbil, A.L. Demirel, Y. Avci, and O. Mert, *Science*, **299**, 1377 (2003).
10. J. Bico, U. Thiele, and D. Quere, *Colloid Surf. A*, **206**, 41 (2002).
11. S. Herminghaus, *Euro. Phys. Lett.*, **52**, 165 (2000).
12. R. Wang, K. Hashimoto, A. Fujishima, M. Chikuni, E. Kojima, A. Kitamura, M. Shimohigoshi, and T. Watanabe, *Nature*, **388**, 431 (1997).
13. K.K.S. Lau, J. Bico, K.B.K. Teo, M. Chhowalla, G.A.J. Amaratunga, W.I. Milne, G.H. McKinley, and K.K. Gleason, *Nano Lett.*, **3**, 1701 (2003).
14. A. Nakajima, K. Hashimoto, and T. Watanabe, *Monatsch. Chem.*, **132**, 31 (2001).
15. D. Quere, *Rep. Prog. Phys.*, **68**, 2495 (2005).
16. X.M. Li, D. Reinhoudt, and M. Crego-Calama, *Chem. Soc. Rev.*, **36**, 1350 (2007).
17. M.L. Ma and R.M. Hill, *Curr. Opin. Colloid Interface Sci.*, **11**, 193 (2006).
18. R. Rioboo, M. Voue, A. Vaillant, D. Seveno, J. Conti, A.I. Bondar, D.A. Ivanovand, and J. De Coninck, *Langmuir*, **24**, 9508 (2008).
19. M. Miwa, A. Nakajima, A. Fujishima, K. Hashimoto, and T. Watanabe, *Langmuir*, **16**, 5754 (2000).

20. A. Marmur, *Langmuir*, **19**, 8343 (2003).
21. A.B.D. Cassie, *Discuss. Faraday Soc*., **3**, 11 (1948).
22. S. Brandon, N. Haimovich, E. Yeger, and A. Marmur, *J. Colloid Interface Sci*., **263**, 237 (2003).
23. L. Gao and T.J. McCarthy, *Langmuir*, **22**, 2966 (2006).
24. N.A. Patankar, *Langmuir*, **20**, 7097 (2004).
25. A. Lafuma and D. Quere, *Nat. Mater*., **2**, 457 (2003).
26. L. Barbieri, E. Wagner, and P. Hoffmann, *Langmuir*, **23**, 1723 (2007).
27. B. He, N.A. Patankarand, and J. Lee, *Langmuir*, **19**, 4999 (2003).
28. R. Rioboo, M. Voue, A. Vaillantand, and J. DeConinck, *Langmuir*, **24**, 14074 (2008).
29. Y.C. Jung and B. Bhushan, *Langmuir*, **24**, 6262 (2008).
30. D. Bartolo, F. Bouamrirene, E. Verneuil, A. Buguin, P. Silberzanand, and S. Moulinet, *Euro. Phys. Lett*., **74**, 299 (2006).
31. M. Callies and D. Quere, *Soft Matter*, **1**, 55 (2005).
32. M. Reyssat, A. Pepin, F. Marty, Y. Chen, and D. Quere, *Euro. Phys. Lett*., **74**, 306 (2006).
33. Y.C. Jung and B. Bhushan, *Langmuir*, **25**, 9208 (2009).
34. B. Liu and F.F. Lange, *J. Colloid Interface Sci*., **298**, 899 (2006).
35. D. Richard, C. Clanet, and D. Quere, *Nature*, **417**, 811 (2002).
36. E. Bormashenko, R. Pogreb, G. Whyman, and M. Erlich, *Langmuir*, **23**, 6501 (2007).
37. X. Yao, Q.W. Chen, L. Xu, Q.K. Li, Y.L. Song, X.F. Gao, D. Quere, and L. Jiang, *Adv. Funct. Mater*., **20**, 656 (2010).
38. M. Nosonovsky and B. Bhushan, *Microelectron. Eng*., **8**, 382 (2007).
39. T.L. Sun, W.L. Song, and L. Jiang, *Chem. Commun*., **24**, 1723 (2005).
40. A.A. Ward and A.I. Khalf, *KGK. Kautsch. Gummi. Kunstst*., **62**, 650 (2009).
41. S.L. Abd-El-Messieh, D.E. El-Nashar, A.F. Younan, and K.N. Abd-El-Nour, *KGK Kautsch. Gummi. Kunstst*., **36–45**, 66 (2013).
42. S. Krumm, *Mater. Sci. Forum*., **228-231**, 183 (1996).
43. N.E. Hill, W.E.Vaughan, A.H.Price, and M. Davies, *Dielectric Properties and Molecular Behavior*, Van Nostrand, London (1969).
44. A.M. Ward, S.H. Mansour, and S.L. Abd-El-Messieh, *J. Appl. Polym. Sci*., **108**, 833 (2008).
45. P.R. Gray, P.J. Hurst, S.H. Lewis, and R.G. Myere, *Analysis and Design of Analog Integrated Circuits*, 5th ed., Wiley, New York 40 (2009).
46. S. George, K.T. Varughese, and S. Thomas, *J. Appl. Polym. Sci*., **73**, 255 (1999).
47. A.K. Jonscher, *Dielectric Relaxation in Solids*, Chelsea Dielectrics Press, London 1983.
48. N.N. Rozik, A.I. Khalaf, and A.A. Ward, *J. Mater. Des. Appl*., **2414–2421**, 31 (2010).
49. A.I. Khalf and A.A. Ward, *Mater. Des*., **31**, 2414 (2010).
50. A.A. Reffaee, A.A. Ward, D.E. El-Nashar, S.L. Abd-El-Messieh, and K.N. Nour, *KGK-Kautsch. Gummi. Kunstst*., **67**, 39 (2014).
51. D.E. El-Nashar, E. Gomaa, and S.L. Abd-Elmessieh, *Polym. Sci. B Polym. Phys*., **47**, 1825 (2009).

 DOI 10.1002/pc